Pi et al. Int J Concr Struct Mater (2021) 15:18
https://doi.org/10.1186/s40069-021-00455-y

International Journal of Concrete Structures and Materials

RESEARCH Open Access

Experimental Study on Basic Mechanical Properties of Core-Column Non-mortar Aerated Concrete Block Masonry

Tianxiang Pi[1,2*], Zhongheng Du[1], Huchen Zhang[1] and Sicheng Wang[1]

Abstract

Autoclaved aerated concrete (AAC) block masonry has been widely used for bearing walls of multi-story buildings or non-bearing walls of high-rise buildings because of its unique advantages, such as lightweight, low pollution output, and excellent thermal insulation performance. However, traditional AAC block masonry has the disadvantages of high water absorption, poor adhesion to mortar, and low construction efficiency. In order to improve the performance of traditional AAC masonry, this paper proposed a new kind of mortar-free AAC block masonry with concrete core-columns. Fundamental mechanical properties of compression and shear were studied. We divided a total of 16 compression specimens into four groups according to different hollow ratios and strength grades of the block, and eight shear specimens into two groups based on different hollow ratios. Each specimen consists of three-layer blocks with two core columns at the point of quadri-section. The diameters of columns were, respectively, 100 mm and 80 mm. The specimens were loaded at a constant speed to evaluate their bearing capacity, displacement response, crack development, and damage state. The formula of the average values and design values of the compressive and shear strength of masonry were obtained statistically. The stress–strain constitutive relation of masonry expressed by a three-stage curve was presented. Furthermore, the result of numerical analysis using the ABAQUS finite element program aligned well with the experimental results. The compressive strength and shear strength of the new type of masonry are no less than traditional AAC masonry, and new masonry has higher construction efficiency and more stable strength.

Keywords: concrete core-column, autoclaved aerated concrete block masonry, compressive strength, shear strength, performance

1 Preface

In recent years, autoclaved aerated concrete(AAC) has been widely used in walls because of its excellent performance of lightweight, sound and thermal insulation, energy-saving, and flexibility (Laukaitis and Fiks 2006; Muszynski and Gulas 2001; Jerman et al. 2013; Laurent and Guerrechaley 1995; Tanner et al. 2005; Ghazi Wakili et al. 2015; Fudge 2011). However, AAC blocks have the disadvantages of poor water retention, mortar fluidity, and strong water absorption capacity (Wittmann 1983). The quality defects in masonry construction are challenging to eliminate, including the plumpness of mortar joint depends heavily on the workers' proficiency, the bond force between mortar and blocks are discrete, the mechanical properties of masonry usually fail to meet the design requirements (Bingel and Bown 2009). Besides, traditional masonry construction is becoming outdated due to its low construction efficiency.

In the dry-stack masonry construction, some measures to improve the performance of masonry structure and construction efficiency have been developed and applied around the world (Sokairge et al. 2017; Zahra and

*Correspondence: pitianxiang@163.com
[1] Chongqing University, Civil Engineering College of Chongqing University, ShaZheng Road 174, Shapinba, Chongqing, People's Republic of China
Full list of author information is available at the end of the article
Journal information: ISSN 1976-0485 / eISSN 2234-1315

Dhanasekar 2018; Fonseca et al. 2019; Bolhassani et al. 2016; Oliveira 2003; Martinez and Atamturktur 2019; Thanoon et al. 2008; Kalliontzis and Schultz 2017; Fay et al. 2014; Zhou et al. 2017; Ngowi 2005). Ngowi (2005) summarized the preliminary development of dry-stack masonry and explored its general failure mode and load capacity. To improve the bearing capacity of dry-stack masonry, Fonseca et al. (2019) used different strength grades of concrete to fill the holes in the blocks and find the disciplinarian of the strength of the grouted masonry. Sokairge, Rashad and Elshafie (Sokairge et al. 2017) conducted a post-tensioning test on the dry-stack masonry to improve crack load and ultimate load. Bolhassani et al. (2016) conducted a partial grouting test on the masonry. In the experiments, the grouted part and the unfilled part formed a frame style structure, and the lateral strength of the masonry was improved. To numerically analyze the mechanical property of grouted masonry, Zhou et al. (2017) proposed the ANN and ANFIS models, which can accurately calculate the shear strength of reinforced masonry. Kalliontzis and Schultz (2017) presented an analysis method to improve the mechanical research of a fully grouted masonry shear wall by accounting for the reverse-cyclic loading and the three mechanisms of rocking, flexure, and shear. Gokmen et al. (2019) investigated the seismic behavior of autoclaved aerated concrete low-rise buildings with reinforced walls according to the relevant ASTM standards (C15.04 2007; C27.60 2009; C15.10 2009).

As stated in reference Fudge (2011), the use of AAC masonry is becoming more and more appealing. To give full play to the mechanical property of masonry structures, the use of reinforced concrete core columns set to confine AAC masonry has been proved effective. When reinforced fiber mesh crammed the vertical gaps between masonry units, higher average compression strength and elasticity modulus could be acquired. Also, when the structural columns have been located in the corners or wall intersections of buildings, both static and shaking table tests showed noticeable improvement of the resistance and ultimate deformation capacity of the walls. Furthermore, the mechanical properties of AAC masonry will be significantly improved by reducing the concrete core-column spacing properly and increasing the number of columns regularly. However, the knowledge regarding their mechanical behavior is still insufficient.

Given the high surface flatness of AAC blocks, a new type of AAC block, with two circular holes at points of the quarter span of the block (Fig. 1), is proposed in this study. The holes of the blocks were made manually by a concrete core drilling machine. Though the blocks were crisp, the drilling process went exceedingly well. Almost all holes of the blocks were successfully drilled without any crack or break. During construction, the holes of the AAC blocks are aligned vertically, and the blocks are staggered to form a dry-stack masonry. Then the high fluidity concrete is poured into the vertical through-holes. Eventually, the cooperation of the core columns and AAC blocks ensures the performance of the masonry. The joints need to be sealed by plastering to guarantee the thermal insulation and waterproof performance of masonry. Since no mortar was used, the masonry structures have many new advantages of reducing pollution on the construction site, accelerating construction, and improving construction quality. The structure of the new masonry, core-column non-mortar aerated concrete block masonry (CNACBM), is shown in Fig. 2.

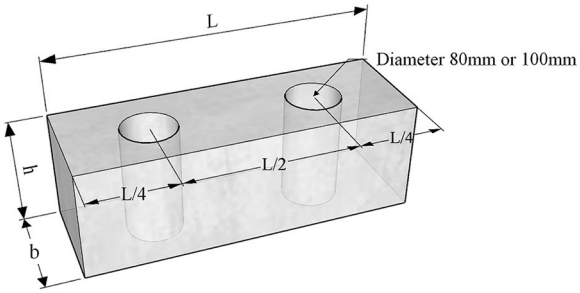

Fig. 1 AAC blocks with holes at quarter span point.

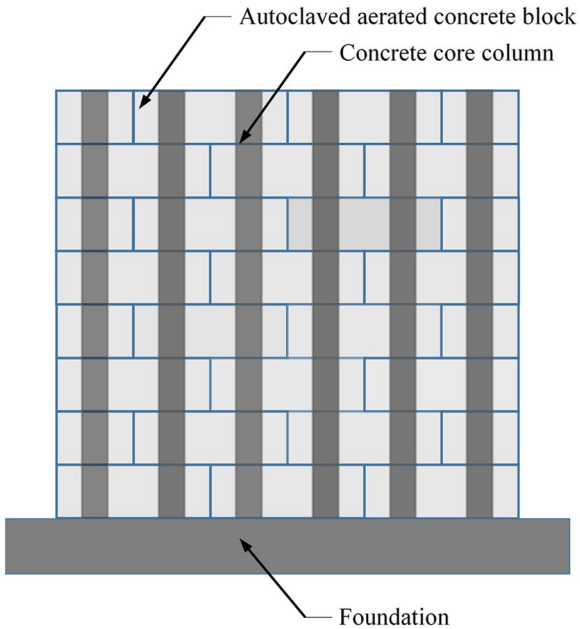

Fig. 2 The wall built in new type of AAC masonry.

This research aims to study the basic mechanical properties of structure units under CNACBM simple working conditions. In order to achieve the purpose, several experimental tests and numerical analyses are performed on both compression and shear specimens, and masonry units' behavior of the crack process and failure characteristics are characterized. Also, the stress–strain relationship of the units and modulus of elasticity were proposed. The results of this research will provide an experimental and theoretical basis for the popularization and application of CNACBM.

2 Test Overview

2.1 Design and Production of the Specimen

2.1.1 Compression Specimen Design

Compression specimens were designed according to Chinese Code JGJ/T 17–2008 (B.I.o.A. Design 2008). The compression tests included two different types of blocks. The dimension of the larger one was 600 (length) × 200 (width) × 200 mm (height) mm^3, while the smaller one was 300 (length) × 200 (width) × 200 mm (height) mm^3. The density of AAC is 500 kg/m^3. The holes in the blocks were connected vertically, as shown in Fig. 3. The AAC blocks were dried at a temperature of 65 ± 5 ℃ for 24 h, then at a temperature of 80 ± 5 ℃ for another 24 h, at last at a temperature of 105 ± 5 ℃ until constant weight. Then we put them in a room with 10% moisture content. The strength of the AAC block was converted into air-dry strength according to reference (Xiangan et al. 2007).

Sixteen compression specimens were divided into four groups according to two strength grades of AAC and two kinds of hole rates. They were named CK1 to CK4. Each group had four specimens numbered CK1-1 to CK4-4. The compressive strength of AAC was tested according to reference (C. Standard 2009). The coefficient of variation of AAC's compressive strength is 0.15, and other mechanical parameters of the concrete and AAC block are shown in Table 1.

The dry-stack specimens were placed on the flat plate, and the blocks were stacked with the holes aligned on a line. Concrete with good fluidity and workability (Eurocode 6 2012; Eurocode 8 2010), which has a slump of 120 mm, was then poured into them and compacted. When the concrete reached its initial setting strength, the uneven surface of the core-column concrete was grounded flat by a grinding wheel machine. Before the test, the actual dimensions of each specimen were recorded.

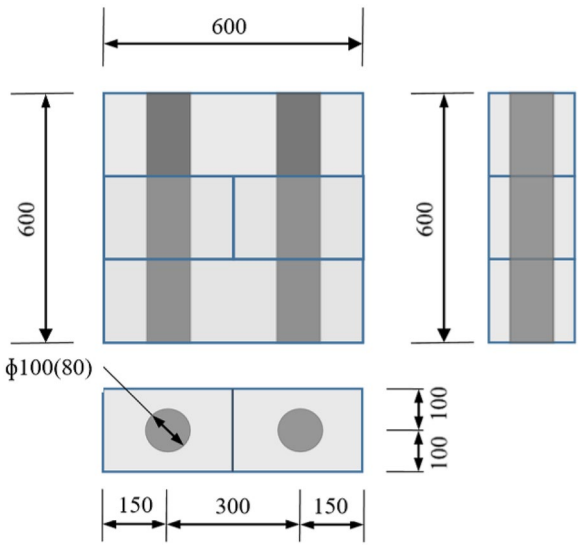

Fig. 3 Masonry specimens for compression tests.

2.1.2 Shear Specimen Design

The shear specimens consisted of two large blocks of 600(L) × 200(W) × 200 mm (H) mm^3 and two small blocks of 300(L) × 200(W) × 200(H)mm^3 in dimensions according to JGJ/T 17-2008 (Association 2008), as shown in Fig. 4. The holes in blocks are vertically connected and aligned, and a 20-mm gap was left between the two small blocks in the middle of the specimen.

A large number of studies revealed that the shear capacity of masonry has little to do with the strength of blocks. Thus only one strength grade of AAC was used in the masonry with hole rates of 13.08% and 8.37% (diameter of 100 mm and 80 mm, respectively). The strength of AAC blocks, with a calibration strength grade of A3.5, was 3.7MPa, which is less than the strength required in EC 8 (Eurocode 8 2010). Eight shear specimens were divided into two groups of SK1 and SK2. Four specimens in each group were named

Table 1 Mechanical parameters of the compression specimens.

Specimen	Concrete compression strength $f_{cu.m}$ [a] (MPa)	Block compressive strength $f_{cc.m}$ [b] (MPa)	Hole rate[c] (%)
CK1	25.48	2.60	13.08
CK2	25.48	2.60	8.37
CK3	25.48	3.70	13.08
CK4	25.48	3.70	8.37

[a] $f_{cu.m}$ is the average strength of core-column concrete measured by standard test method.

[b] $f_{cc.m}$ is the average strength of block measured by reference (GB/T11969-2008).

[c] Calculated by the sum of the two hole areas to the cross-sectional area of the test piece.

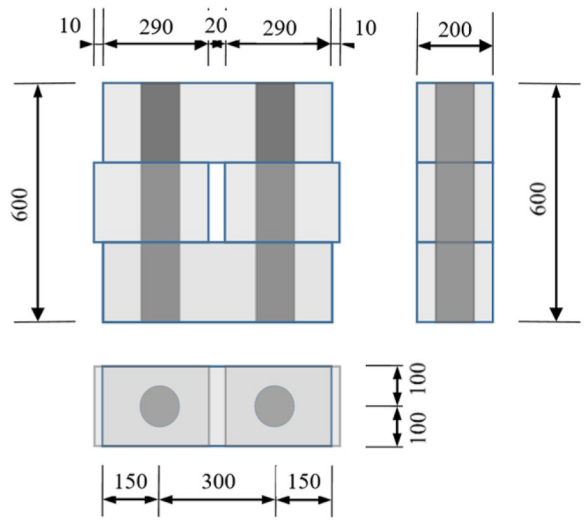

Fig. 4 Masonry specimens for shear tests.

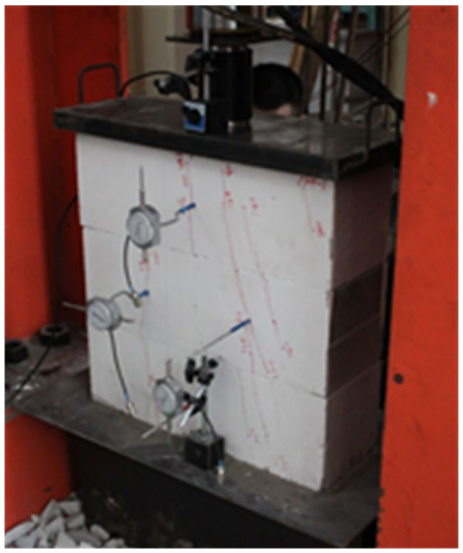

Fig. 5 Compression test device.

Table 2 Mechanical parameters of the shear specimens.

Specimen	Concrete compression strength f_{cu} (MPa)	Block compressive strength f_{cc} (MPa)	Hole rate[c] (%)
SK1	24.56	3.70	13.08
SK2	24.56	3.70	8.37

SK1-1 to SK2-4, respectively. The main parameters of the specimens are shown in Table 2.

2.2 Test Equipment and Measurement Scheme

2.2.1 Compression Test Procedures

The experiments were carried out in the structural laboratory at Chongqing University's School of Civil Engineering. Details of the test setup, loading system, and instrumentation are shown in Fig. 5. The I-beam foundation of test specimens was anchored to the laboratory's strong floor. A capacity of 1000 kN of the hydraulic actuator was fixed upside down on the reaction beam of the steel frame. The specimens with a thickness of 40-mm steel plate on the top surface were set between the foundation and the door-type steel support, while a pressure sensor was set on the top of the plate. In order to record the deformation behavior in compression, percentiles were installed on horizontal and vertical centerlines of the side of the specimen.

The loading system was to apply 5 to 10% of the estimated failure load and 3 to 5 times at first to check whether the test device worked normally, then the specimens were loaded at a uniform rate of 10% the expected failure load, and each loading stage was held for 60 to 90 s. At the interval, the percentile and pressure sensor values were recorded instantly.

Fig. 6 Shear test device.

The experimental data on pressures and deformations were recorded uninterruptedly by high-speed cameras. The camera was aligned with the force sensor display and three dial gauges, and a set of data was recorded for each shot. This method improved efficiency and eliminated the asynchrony of manual meter recording. More importantly, it can fully record the load and deformation data of the specimens even at the failure stage, to achieve the full load-deformation curve reliably.

2.2.2 Shear Test Procedures

The details of the shear test device are shown in Fig. 6. The shear test device was the same as in the compression test. The shear specimens were turned 90 degrees and placed on the foundation so that the horizontal joints were vertical to the plate. The upper pressing plate was placed on the top of the specimens. The hydraulic actuator, fixed on the reaction frame, was adopted

for loading. To get universal and basic properties of masonry units instead of the whole masonry wall, we designed the test without the lateral compression force according to Standard for test method of basic mechanical properties of masonry, chapter 5 (GB/T 50129-2011) (I.a.Q.o.t.P.s.R.o.C 2011) and Technical specification for application of autoclaved aerated concrete, appendix D (JGJ/T 17-2008) (Technical specification 2008).

The loading process was slow and uniform at a constant speed of 1 ~ 2kN/s, according to reference (B.I.o.A. Design 2008). The maximum load occurred when either concrete core-column was broken near the joints of masonry, and then the loading was stopped, and the maximum load was recorded.

3 Experiment Phenomena and Results

3.1 Pressure Test Phenomenon and Mechanism

The failure process of the CNACBM specimens under compression can be roughly divided into four stages: elastic stage, crack occurrence, crack development, and masonry failure. Before the first crack appeared, the blocks had a perfect bond with the core columns, and the masonry was nearly in an elastic state. The force diagram of the block is shown in Fig. 7. Then the first visible crack appeared on the surface of the AAC block near core columns. Under the uniform pressure, the negative moment at the sections of the block near the columns cannot be ignored. Besides, the block sections are weakened by the holes. So the first vertical crack of the masonry usually appears here. Researches have revealed the high brittleness properties of AAC (Trunk et al. 1999; Małyszko et al. 2017), which determines that the masonry cracking load is relatively low, being about 15–30% of the ultimate load as shown in Table 3.

With the increase of the load, the cracks developed symmetrically along with the blocks, while the stiffness of the masonry experienced a continuing decline. When approaching the peak load, the vertical cracks on the surface of AAC blocks near both sides of the core columns extended and penetrated, forming the prominent cracks. At the peak load, the cracks promptly increased in number and quickly widened and deepened. Some fragments on the surface of blocks fell, then the specimen was unloaded rapidly. It was observed that the specimen was divided into several short columns by the cracks and the two core columns crushed after removing the fragments of blocks, as shown in Fig. 8. The compressive strengths of the CNACBM specimens are recorded in Table 3.

3.2 Shear Test Phenomenon and Mechanism

The test phenomena of eight shear specimens are the same. The first crack appeared on the surface of blocks near core columns when the load approached the ultimate load. The moment the first crack appeared, the load dropped to 80% of the ultimate load. Then the load re-stabilized as the load continued. The cracks on both sides became more in-depth and more extensive, and the horizontal cracks of some specimens developed to the intermediate block. Due to the lack of lateral restraint, the blocks on both sides bent in-plain. The cracks in these blocks were widened. Finally, when the concrete on one side of the column broke, the specimen was utterly ineffective, and the load was lower

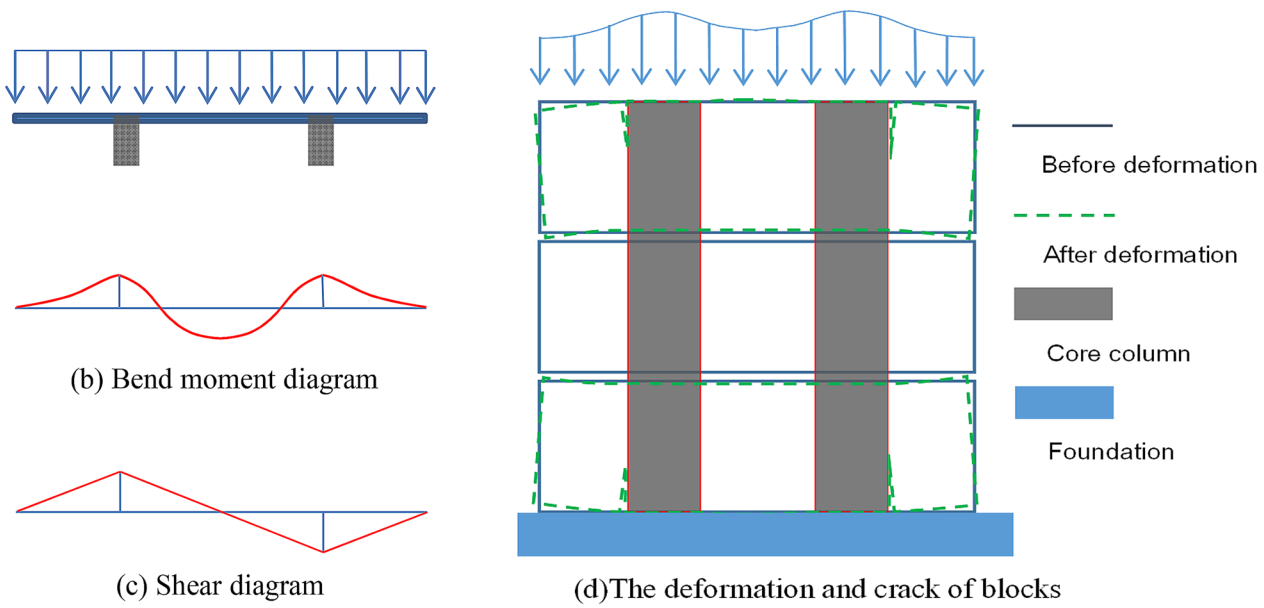

Fig. 7 Force mechanism of the compression specimen.

Table 3 Test results of compressive strength of masonry specimens.

Specimen	Measured size of specimen		Cracking load (kN)	Failure load (kN)	Compressive strength f_{cu} (MPa)	Average compressive strength f_{cu} (MPa)	Coefficient of variation
	Length (mm)	Width (mm)					
CK1-1	596	199	90	290.4	2.42	2.36	0.15
CK1-2	598	199	80	264.3	2.20		
CK1-3	596	198	30	340.1	2.83		
CK1-4	595	198	30	239.2	1.99		
CK2-1	596	200	25	225.0	1.87	1.95	0.15
CK2-2	595	199	30	282.4	2.35		
CK2-3	596	198	50	227.1	1.89		
CK2-4	594	198	50	200.4	1.67		
CK3-1	596	199	20	241.3	2.01	2.80	0.18
CK3-2	594	199	30	336.8	2.81		
CK3-3	595	199	90	399.0	3.32		
CK3-4	595	199	50	365.4	3.04		
CK4-1	596	198	60	263.8	2.20	2.37	0.18
CK4-2	595	198	65	364.4	3.04		
CK4-3	598	199	30	260.1	2.17		
CK4-4	594	198	80	251.0	2.09		

than the load when the crack occurred. Figures 9 and 10 show the crack development and failure mode of the shear specimens. The shear test results of the specimens are shown in Table 4.

The core columns in the specimen bore all the section shearing force. Before the block crack occurred, the concrete core-columns were in a pure shear force state, and their shear capacity was relatively strong at this time. However, since the test employed top-loading on the middle block, and the load was transmitted through the core columns to the blocks on both sides, the finite rigidity of the core column caused the eccentric pressure to be formed in the outer block, thereby cracking the outer block surface. Moreover, the horizontal cracks on blocks developed quickly, which in turn caused sizable bending deformation in the concrete core-columns. The concrete core-columns eventually broke under the combined action of shear force and bending moment. Under the influence of a nonnegligible shear span rate, the shear capacity of the concrete core-column was smaller than the masonry without cracking.

4 Analysis of Test Results

4.1 Calculation of Compressive Strength

4.1.1 The Average Value of Compressive Strength f_{gm}/MPa

Since the external load is shared by the blocks and the core columns of the CNACBM together, the compressive strength of the masonry is composed of the block strength part and the concrete core-column part. We assume that there exists a gap between AAC blocks because of the dry-stack construction method and the unevenness of AAC blocks' surface, which causes a displacement before the blocks fully contact.

Taking consideration the fact that the masonry would not break until the core columns reached its ultimate strain about 0.002 under axial force, while the strain of the AAC blocks remained a small value because of the gaps, the strength of the block part can be expressed as follows:

$$f_{cc} = f_{cc,m} \times \left[1.3 \times \frac{\varepsilon}{\varepsilon_p} - 0.3 \times \left(\frac{\varepsilon}{\varepsilon_p}\right)^3\right] \quad (1)$$

Referring to the formula form of grout for the AAC hollow block in GB 50003–2011 (C. Standard 2012), the compressive strength of CNACBM is expressed as follows:

$$f_{gm} = k_1 k_2 \alpha f_{cu,m} + (1-\alpha) f_{cc}, \quad (2)$$

where $f_{cc,m}$=the average value of compressive strength of aerated concrete cube specimen; ε=the actual strain of aerated concrete cube specimen; ε_p=the ultimate strain of aerated concrete cube specimen; f_{gm}=the average value of the compressive strength of CNACBM; $f_{cu,m}$=the average value of concrete axial compressive strength; f_{cc}=the actual compressive strength of aerated concrete cube specimen; α=the

(See figure on next page.)

Fig. 8 Crack developent and failure pattern of compressive specimens.

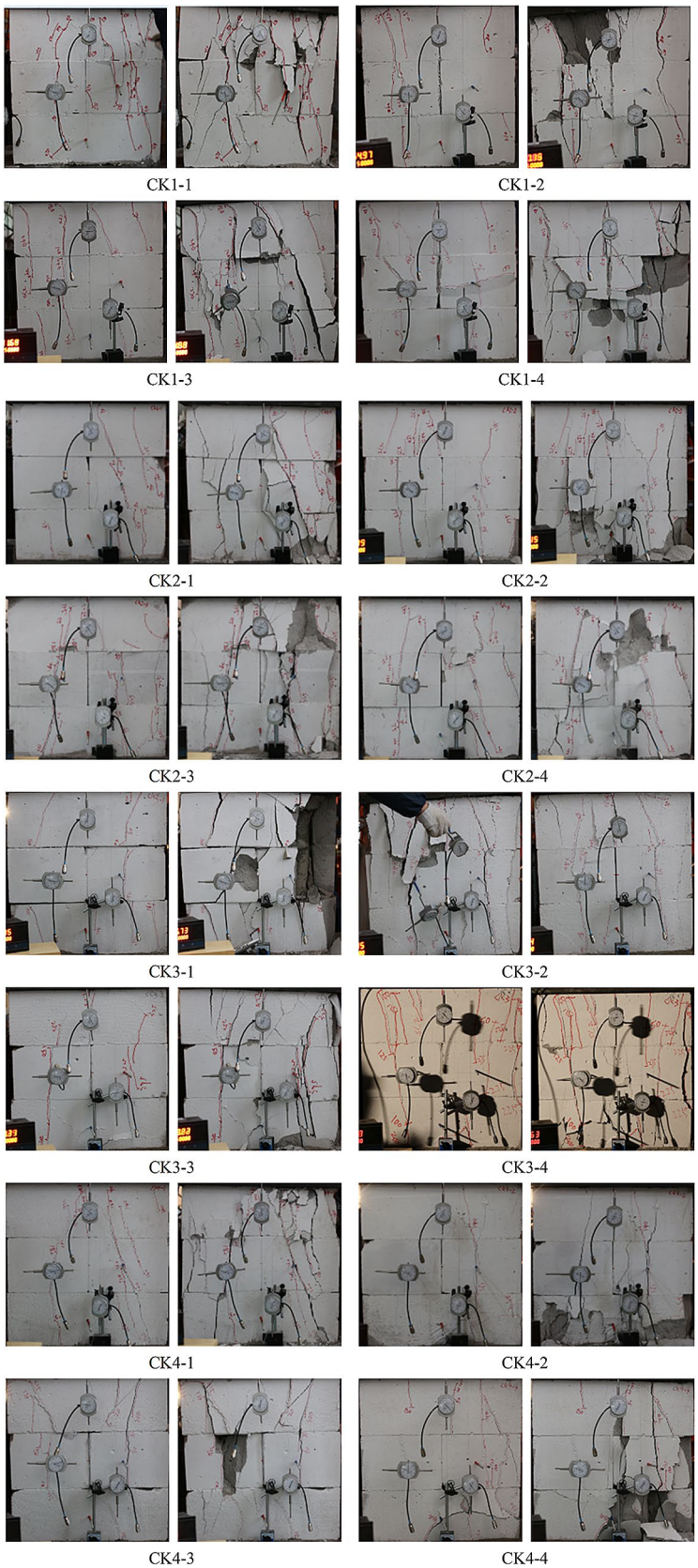
CK1-1
CK1-2
CK1-3
CK1-4
CK2-1
CK2-2
CK2-3
CK2-4
CK3-1
CK3-2
CK3-3
CK3-4
CK4-1
CK4-2
CK4-3
CK4-4

Fig. 9 Core-column concrete failure.

void ratio of the area of the void to the area of the gross; k_1 are the insufficient coefficient of concrete strength and AAC block strength; k_2 is the ratio of axial compressive strength to cube compressive strength of concrete, $k_2 = 0.67$ C. Standard 2011).

The test results showed that the following three factors limited the strength of the core columns in the masonry: (1) it was difficult to achieve accurate vertical alignment of the blocks' hollow during construction, which reduced the effective cross-sectional compression area of concrete core-columns; (2) when loading pressure on the masonry, the two concrete core-columns could not reach the ultimate compressive strength at the same time; (3) after the splitting of the core column, the blocks lost restraint function on the concrete core-column, and the core column became a long column with a greater slenderness rate. Based on the above factors, the compressive strength of the concrete core-column can be multiplied by the reduction factor of 0.9 based on the ultimate compressive strength of the concrete. $k_1 = 0.9$ can be obtained after regression processing, and the calculation formula of the average compressive strength of the CNACBM is

$$f_{gm} = 0.6\alpha f_{cu,m} + (1-\alpha) f_{cc,m} \times \left[1.3 \times \frac{\varepsilon}{\varepsilon_p} - 0.3 \times \left(\frac{\varepsilon}{\varepsilon_p}\right)^3\right], 0 \leqslant \frac{\varepsilon}{\varepsilon_p} \leqslant 1 \quad (3)$$

The main factors affecting the mechanical properties of new masonry are the mechanical index of concrete and aerated concrete block, block size, void ratio, etc. In this test, ordinary strength concrete and aerated concrete block are applied. The length–width ratio of the block is about 3, and the void ratio is between 7.3 and 13.8%. Before more effective test and analysis data are available, masonry parameters should not exceed the range of existing test parameters when the formula is applied safely.

Table 5 lists the average values of the masonry's compressive strength, which are calculated by Formula (3) and the measured test values. The calculated values and the measured values are close, indicating that the proposed formula aligns well with the test results.

4.1.2 Design Value of Compressive Strength f_g/MPa

After the consideration of the reliability requirements of masonry structures, the design value of the compressive strength of CNACBM is obtained as follows by GB50003-2011 C. (Standard 2012):

$$f_g = \left[0.6\alpha f_{cu,m}(1 - 1.645\delta_c) + 0.26(1-\alpha) f_{cc,m}(1 - 1.645\delta_f)\right] / \gamma_f, \quad (4)$$

where δ_c, δ_f are the coefficient of variation of concrete strength and AAC strength, respectively, $\delta_c = 0.12$ and $\delta_f = 0.15$ (Standard 2011) as stated above; γ_f is a partial safety factor for the property of masonry, $\gamma_f = 1.6$ (C. Standard 2012). That is

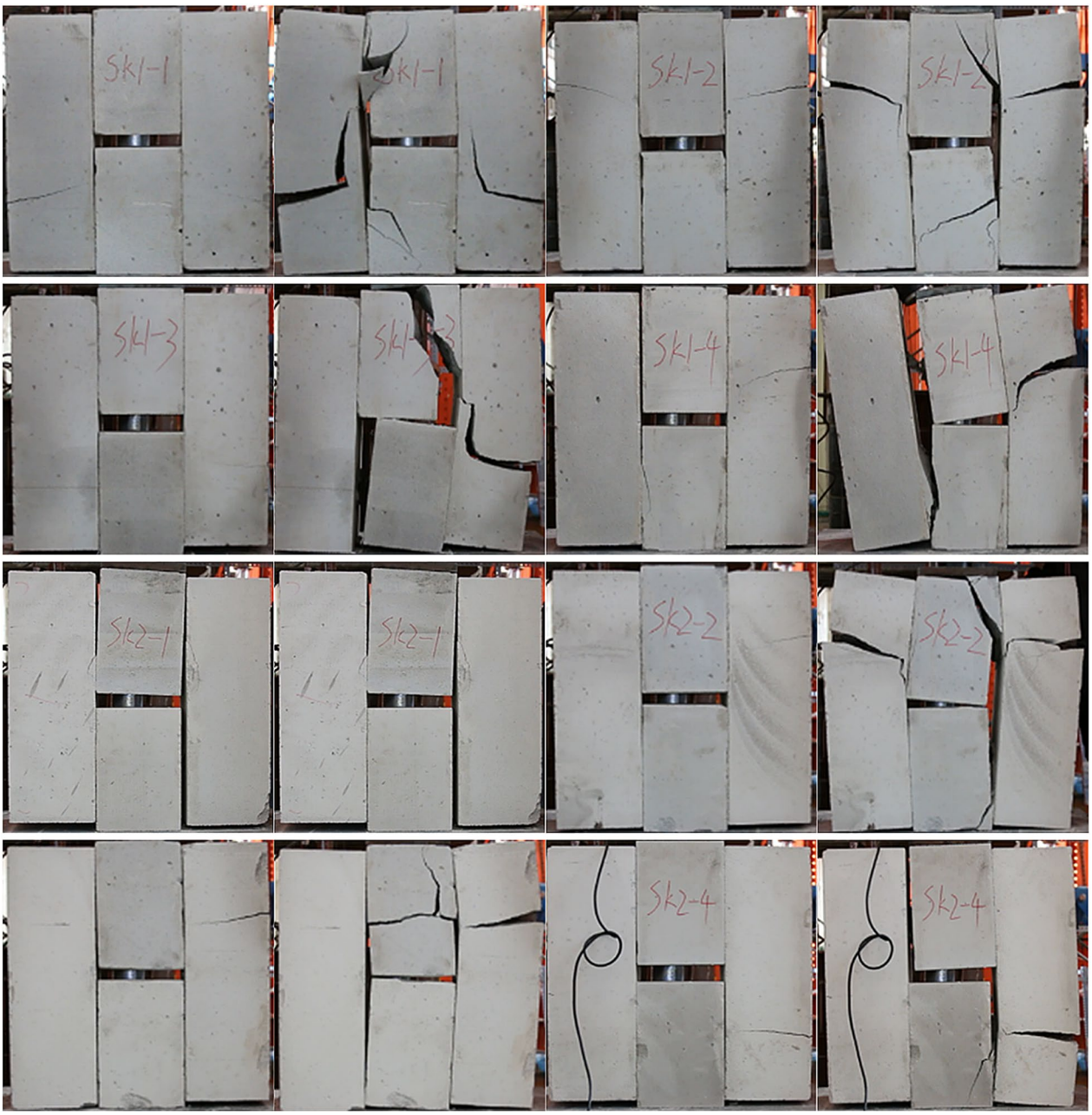

Fig. 10 Development and failure pattern of sheared specimen.

$$f_g = 0.32\alpha f_{cu,m} + 0.13(1-\alpha)f_{cc,m}, \quad (5)$$

where f_g is the design value of masonry compressive strength (MPa).

The design values of the masonry compressive strength calculated by Formula (5) and the values specified in the literature (B.I.o.A 2008) are shown in Table 6. Most of the design values of the compressive strength of the CNACBM specimens are larger than that of the AAC masonry except for the specimen, which has a lower void ratio and concrete strength grades at the same time.

4.2 Performance of Compressive Deformation

4.2.1 Compressive Stress–Strain Curve

The compressive strain under static load can be determined by using the dial gauge to record the longitudinal deformation between the measured points of the

Table 4 Test values and average values of masonry shear strength.

Specimen	Failure load (kN)	Shear strength f_{cu} (MPa)	Average shear strength f_{cu} (MPa)	Coefficient of variation
SK1-1	14.91	0.12	0.12	0.20
SK1-2	9.89	0.08		
SK1-3	18.31	0.15		
SK1-4	13.86	0.12		
SK2-1	10.43	0.09	0.07	0.16
SK2-2	8.57	0.07		
SK2-3	7.90	0.07		
SK2-4	7.27	0.06		

specimens. According to the test results, the stress and strain values of the specimen under the static load were obtained and normalized. A constitutive relation model similar to that proposed by Zhenhai (1999) is adopted. The three-section equation is used to describe the characteristic of the stress–strain curve. Before the masonry cracks, it is basically in the elastic stage, and its stress–strain curve is expressed as a straight line. When approaching the falling section of the stress–strain relationship, the quadratic parabola with different parameter values is used to fit the curve, respectively, and the curve at each characteristic point should be smooth. The stress–strain equation is shown in Formula (6). The average peak compressive strain ε_0 in the formula obtained from the test results of the 15 sets of specimens is 0.0093, and the coefficient of variation is 0.22. σ_0 is the peak compressive stress. Figure 11 shows that the fitting curve is in good agreement with the standardized stress–strain relationship measurement points of the CNACBM specimens.

Table 5 Comparison of measured values to compressive strength with formula values (MPa).

Specimen	α (%)	$f_{cu.m}$ (MPa)	f_{cc}	$\frac{\varepsilon}{\varepsilon_p}$	$f_{g.m}^{0}$ [a]	$f_{g.m}$ [b]	$f_{g.m}^{0}/f_{g.m}$
CK1	13.08	25.48	2.60	0.00033	2.36	2.52	0.94
CK2	8.37	25.48	2.60	0.00033	1.95	1.82	1.07
CK3	13.08	25.48	3.70	0.00033	2.80	2.73	1.03
CK4	8.37	25.48	3.70	0.00033	2.37	2.03	1.17

[a] $f_{g.m}^{0}$ is the average value of the measured compressive strength of the masonry.

[b] $f_{g.m}$ is the average value of the calculated compressive strength of the masonry.

Table 6 Comparison of recommended values with regulatory values (MPa).

Specimen	Hole rate (%)	Concrete strength class	AAC compressive strength class	Calculated value	JGJ/T 17-2008 value (Technical specification 2008)	
					Mortar ≥ M5	Mortar = M2.5
CK1	13.08	C25	A2.5	1.37	0.98	0.67
CK2	8.37	C25	A2.5	0.73		
CK3	13.08	C25	A3.5	1.45	0.97	0.9
CK4	8.37	C25	A3.5	1.06		

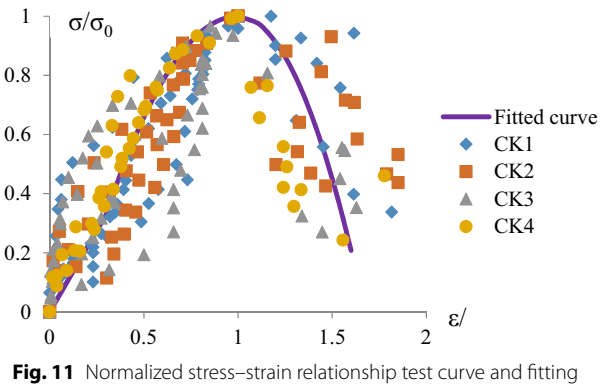

Fig. 11 Normalized stress–strain relationship test curve and fitting curve.

$$\frac{\sigma}{\sigma_0}=\begin{cases}1.1\frac{\varepsilon}{\varepsilon_0} & \frac{\varepsilon}{\varepsilon_0}\leqslant 0.30\\ -1.37\left(\frac{\varepsilon}{\varepsilon_0}\right)^2+2.73\frac{\varepsilon}{\varepsilon_0}-0.37 & 0.30<\frac{\varepsilon}{\varepsilon_0}\leqslant 1.0\\ -2.2\left(\frac{\varepsilon}{\varepsilon_0}\right)^2+4.4\frac{\varepsilon}{\varepsilon_0}-1.2 & \frac{\varepsilon}{\varepsilon_0}>1.0\end{cases} \quad (6)$$

Table 7 Elastic modulus of CNACBM.

Specimen grouping	Elastic modulus (MPa)	E/f_{gi}	Average value of E/f_{gi}	Coefficient of variation
CK1-1	415.95	172.78	701.27	0.77
CK1-2	2767.50	1258.72		
CK1-3	420.42	148.52		
CK1-4	2436.34	1225.07		
CK2-1	626.67	335.00	335.82	0.51
CK2-2	381.33	154.23		
CK2-3	328.40	173.90		
CK2-4	1127.29	680.15		
CK3-1	1880.74	937.17	311.06	0.84
CK3-2	407.76	145.52		
CK3-3	265.91	80.15		
CK3-4	247.51	81.39		
CK4-1	807.46	368.03	235.57	0.37
CK4-2	453.81	149.67		
CK4-3	—	—		
CK4-4	394.61	189.03		

Table 8 Comparison of measured shear strength and formula value (MPa).

Specimen	α (%)	$f_{cu.m}$ [a]	$f^0_{vg.m}$ [b]	$f_{vg.m}$ [c]	$f^0_{vg.m}/f_{vg.m}$
SK1	13.08	24.56	0.12	0.113	1.05
SK2	8.37	24.56	0.07	0.072	0.92

[a] $f_{cu.m}$ is the average value of measured concrete strength.

[b] $f^0_{vg.m}$ is the average value of measured masonry shear strength.

[c] $f_{vg.m}$ is the value calculated by Formula (9).

transferred sufficiently through vertical blocks owing to the gaps between blocks, and this may cause large deformations in the top and bottom blocks. Also, the test results are more discrete.

Regression analysis is performed on the measured values of the elastic modulus in Table 7. The elastic modulus of the CNACBM expressed by the masonry strength design value E/f_g can be calculated as follows:

$$E = 937 f_g. \tag{7}$$

4.3 Shear Characteristic Strength

The shear strength of CNACBM is mainly determined by the concrete core-columns. It can be calculated according to the experiment conducted by Zhenhai (1999), in which the calculation formula of the average concrete shear strength can be obtained by the direct shear test of the short rectangular concrete beams. That is,

$$f_{vc} = k\sqrt{f_c f_t}, \tag{8}$$

where f_{vc} is the shear strength of concrete (MPa); k is correction factor; f_c is compression strength of concrete (MPa) and f_t is the tensile strength of concrete (MPa).

According to the measured test data, the regression analysis is performed on the parameter k. The average shear strength is calculated as follows:

$$f_{vg,m} = 0.06\alpha f^{5/6}_{cu,m}. \tag{9}$$

Due to the lack of lateral restraint in the shear test, the limitation of the proposed formula also includes the load condition of lateral restraint. The measured values of the test and the average values proposed by Formula (9) are listed in Table 8, which shows that the average compressive strengths of masonry calculated according to Formula (9) align well with the measured values.

The coefficient of variation of the compressive strength of the CNACBM is 0.17, and the partial material coefficient is 1.6. The shear strength design value f_{vg} of the masonry expressed by the design value of concrete strength f_c is as follows (Huchen 2017):

Table 9 Comparison of recommended values and regulatory values.

Specimen	Hole rate (%)	Strength grade of concrete	Strength grade of block	Calculated value	Regulatory value	
					Strength grade of mortar ≥ M5	Strength grade of mortar = M2.5
SK1	13.08	C25	A3.5	0.06	0.05	0.03
SK2	8.37	C25	A3.5	0.05		

4.2.2 Elastic Modulus

The elastic modulus of the CNACBM is taken from the secant modulus of the stress–strain curve. Eurocode 6 (2012) proposes to evaluate the elastic modulus through a linear relationship with the masonry characteristic compressive strength. Table 7 shows the rate of the elastic modulus and masonry strength test value for each specimen.

Compared with traditional AAC masonry, the CNACBM is inferior in elastic modulus because, in the initial stage of the loading process, the loads cannot be

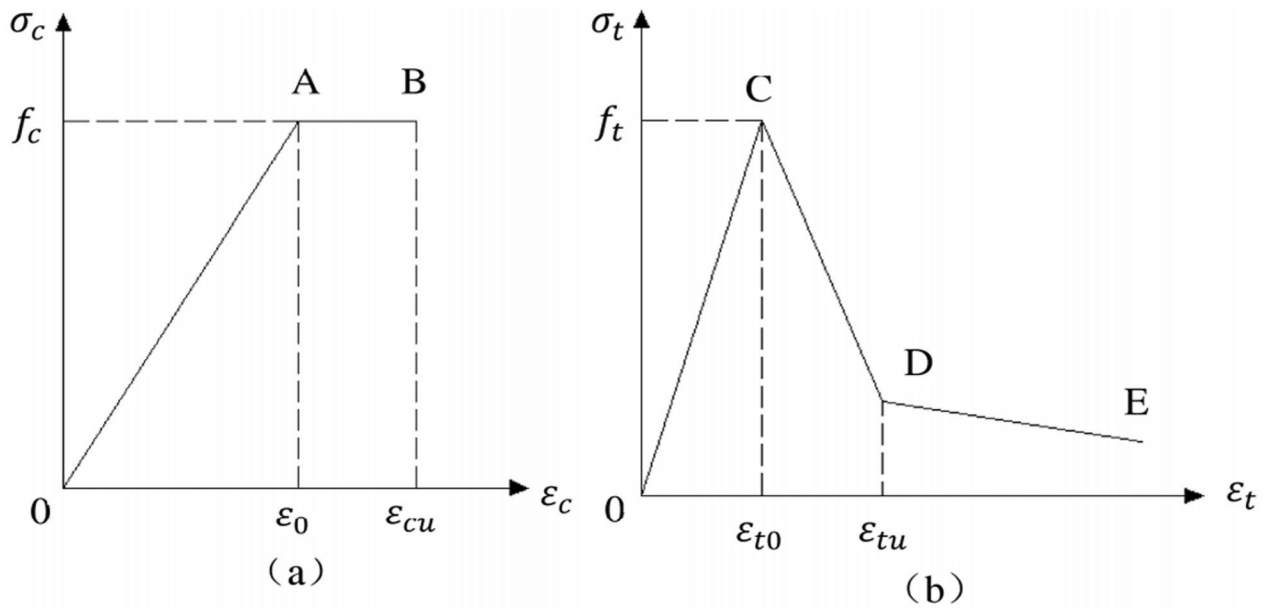

Fig. 12 Constitutive relation of autoclaved aerated concrete.

$$f_{vg} = 0.06\alpha f_c^{5/6}. \tag{10}$$

The design value of the masonry shear strength calculated by the recommended Formula (10) is compared with the design value in the technical specification of autoclaved aerated concrete (Martinez and Atamturktur 2019), and Table 9 is obtained:

The shear strength of both types of CNACBM in Table 9 is not lower than that of traditional AAC masonry, whose mortar strength is not less than that of M5 in the masonry structural engineering stipulations (Martinez and Atamturktur 2019).

5 Finite Element Analysis of Masonry Compression and Shear Performance

5.1 Analysis of Compression Performance of Specimens

According to the failure process of the compression specimens mentioned above, it can be seen that at the early stage of the loading process, the concrete core-columns had good adhesion to the AAC blocks, and the concrete core-columns carried most of the axial pressure. Meanwhile, due to the uneven surfaces of the AAC block and the dry-stack method, the surfaces of the block were not fully contacted, so the axial force transmitted through the blocks was relatively small. With the increase of the compression deformation of the concrete core-columns, especially after the cracks appeared on AAC blocks under the simultaneous effect of the pressure and the bending moment, the contact between the blocks became tight, and the proportion of bearing axial force by the blocks increased. When the concrete core-column broke, the masonry first reached the ultimate compressive strain, and the AAC blocks were then crushed by the splitting.

The finite element analysis model of the CNACBM is highly nonlinear (Martinez and Atamturktur 2019). It includes the nonlinear stress–strain constitutive relationship (with considerable differences between ordinary concrete and aerated concrete), the nonlinear contact relationship between the horizontal and vertical surfaces of the blocks, and the bond between the concrete core-column and the block. To accurately reflect the force mechanism of CNACBM under compression, the ABAQUS finite element model is established according to the following main features of masonry stress:

(1) The regulations (JGJ/T 17-2008) (C.A.C. Association 2008) stipulate that the surface roughness of AAC blocks should not exceed 1 ~ 3 mm. It is challenging to accurately quantify the gap width between the blocks in the masonry because it is affected by the surface flatness and construction conditions. Therefore, in this finite element analysis model, it is assumed that the block gap width is uniformly 0.5 mm. When the pressure reduces the gap width to less than 0.5 mm, the two blocks begin to contact and transmit force.

(2) There is an assumption that the concrete core-columns and the AAC blocks have good adhesion during the whole loading process, which is consistent with the bearing characteristics of the masonry before the masonry reaches peak stress. It can better simulate both the mechanical properties of the masonry in

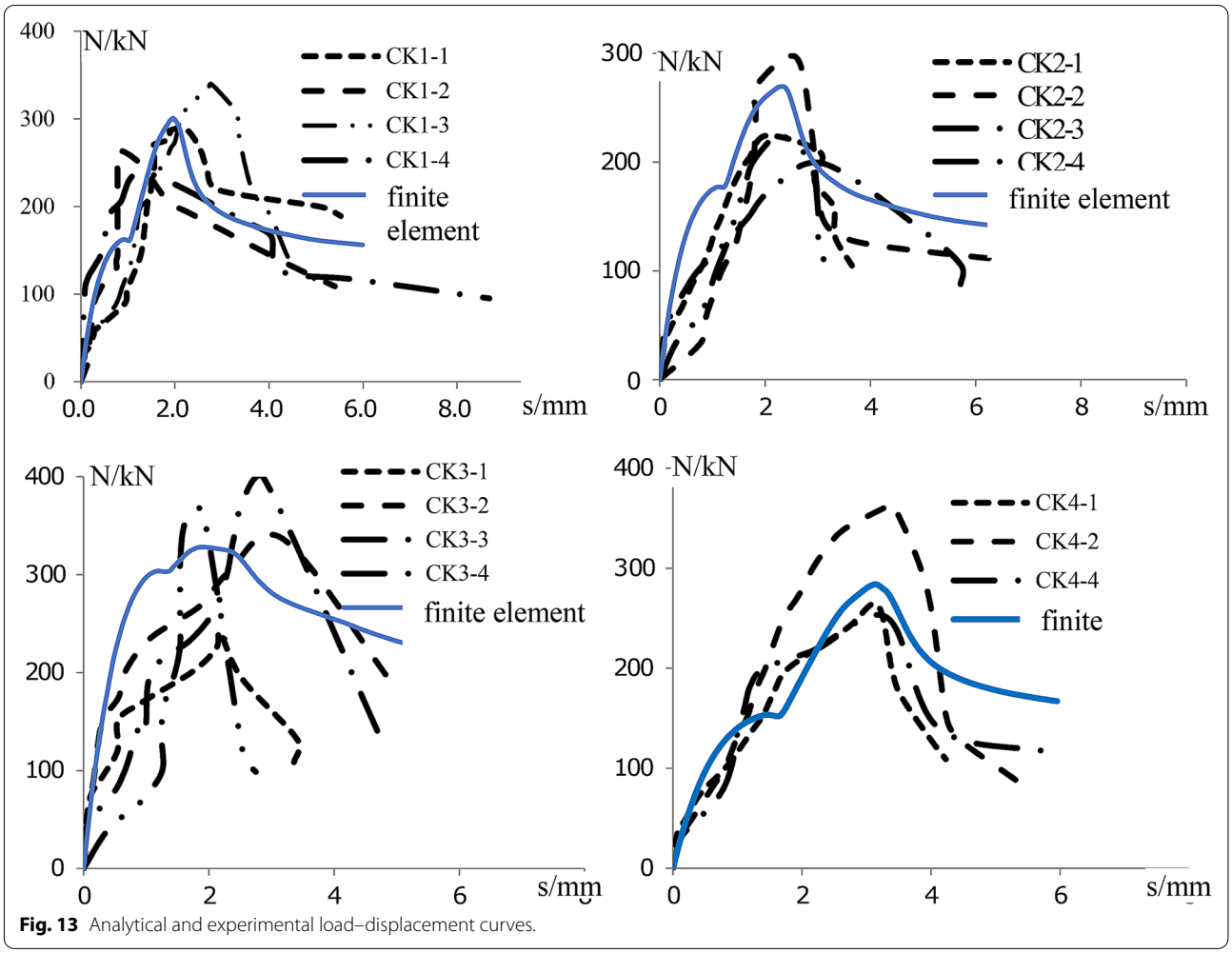

Fig. 13 Analytical and experimental load–displacement curves.

Table 10 Comparison of finite element analysis and experimental results (kN).

Specimen	$F_{max,a}$	$F_{max,t}$	$F_{max,a}/F_{max,t}$
CK1	300.51	283.50	1.06
CK2	269.46	233.73	1.15
CK3	328.11	335.60	0.98
CK4	288.82	296.10	0.96
SK1	15.46	14.24	1.08
SK2	9.22	8.54	1.08

$F_{max,a}$ maximum load in finite element analysis.

$F_{max,t}$ average maximum load in the experiment.

the early stage of the loading process and the bearing capacity of the specimen. However, the conformity of the assumption is slightly weak in the later stage.

(3) Both the core-column concrete and the aerated concrete adopt the plastic damage model of concrete with smeared cracking. The damage plasticity model of AAC material was adopted from Technical Specification for Application of Autoclaved Aerated Concrete (B.I.o.A. Design 2008) as shown in Fig. 12, while the damage parameter was calculated according to reference (Zhang et al. 2008) as shown in Formula (11). According to ref (B.I.o.A. Design 2008), $\varepsilon_{t0} = 150 \times 10^{-6}, \sigma_D = 0.25 f_t, \varepsilon_D = 300 \times 10^{-6}, \sigma_E = 0.02\ Mpa, \varepsilon_D = 1200 \times 10^{-6}$. The concrete damage plasticity model and damage parameter of concrete were adopted from Code for design of concrete structures, Appendix C (C. Standard 2011). The uniaxial compression and tensile stress–strain constitutive relationship of ordinary concrete adopt the Formula recommended by the Code for Design of Concrete Structures (C. Standard 2011). The aerated concrete adopts the Formula recommended by Zhenhai (1999). They are, respectively, Formulas (12) and (13).

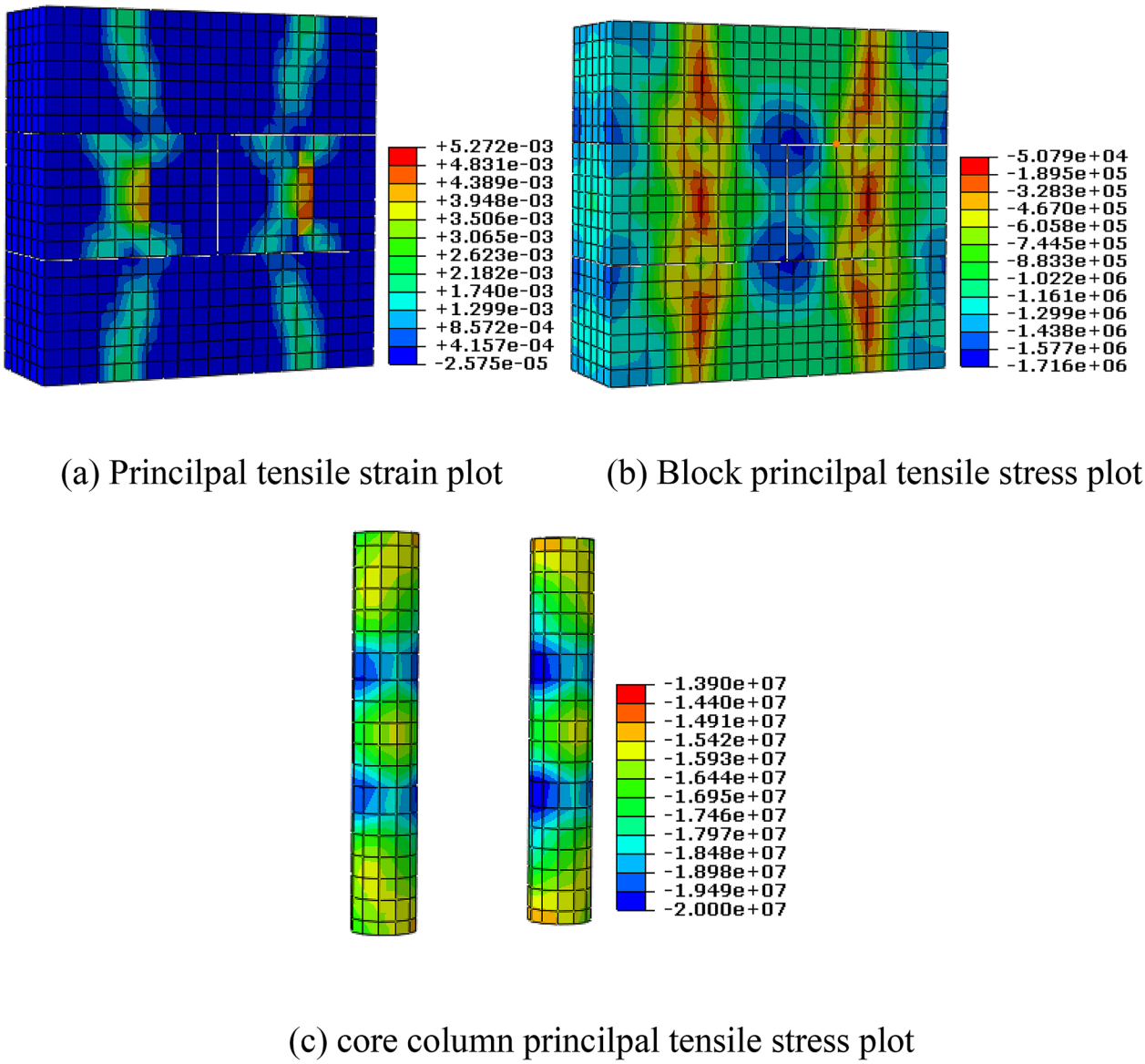

Fig. 14 Stress–strain plot of the peak load of CK1-1 specimen.

$$d_k = \frac{(1-\beta)\varepsilon_k^{in} E_0}{\sigma_k + (1-\beta)\varepsilon_k^{in} E_0}, (k = c, t), \tag{11}$$

where c, t = compression, tensile; d_k = damage factor; σ_k != stress corresponding to strain; E_0 = initial undamaged elastic modulus; ε_k^{in} = inelastic strain; β = the scale factor, 0.6 in compression and 0.9 in tension.

The uniaxial compression constitutive relation of AAC is

$$\frac{\sigma}{f_p} = \begin{cases} 1.3\frac{\varepsilon}{\varepsilon_p} - 0.3(\frac{\varepsilon}{\varepsilon_p})^3 & \frac{\varepsilon}{\varepsilon_p} \leqslant 1 \\ (1 - 1.2\frac{\varepsilon}{\varepsilon_p})/(3.5 - 3.7\frac{\varepsilon}{\varepsilon_p}) & \frac{\varepsilon}{\varepsilon_p} > 1 \end{cases} \tag{12}$$

where f_p is the prismatic strength of autoclaved aerated concrete and ε_p is the corresponding peak strain, $\varepsilon_p = 0.002$.

The uniaxial tensile constitutive relation of autoclaved aerated concrete is

$$\frac{\sigma}{f_t} = \begin{cases} 1.2\frac{\varepsilon}{\varepsilon_t} - 0.2(\frac{\varepsilon}{\varepsilon_t})^6 & \frac{\varepsilon}{\varepsilon_p} \leqslant 1 \\ \frac{\varepsilon/\varepsilon_t}{\alpha_t(\varepsilon/\varepsilon_t - 1)^{1.7} + \varepsilon/\varepsilon_t} & \frac{\varepsilon}{\varepsilon_p} > 1 \end{cases} \tag{13}$$

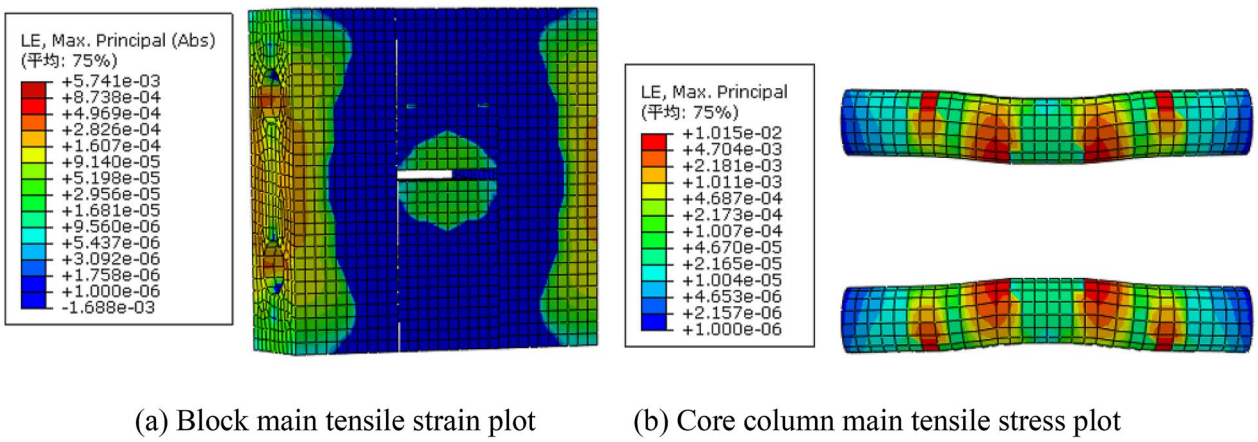

Fig. 15 Strain plot of SK1 specimen under peak load.

In the above Formula, $\alpha_t = 0.312 f_t^2$, f_t is the uniaxial tensile strength of concrete, ε_t is the peak tensile strain corresponding to f_t,$\varepsilon_t = (1500 + 200 f_p^{0.5}) \times 10^{-6}$.

(4) The contact model uses hard contact between the blocks and takes the coefficient of friction as 0.3. The tangential direction does not include friction.

The load–displacement curves of specimens CK1-CK4 were analyzed by ABAQUS finite element program, as shown in Fig. 13. It shows some dispersion between the load–displacement relationship of each specimen, and the analysis results reflect the average condition of each specimen in the overall loading process. The comparison of maximum loads of finite element analysis and experiment averages is shown in Table 10. As can be seen in the table, the rate of the analytical value to the experimental value aligns well with the test results.

Figure 14 shows the typical stress and strain distribution pattern of the specimen CK1-1 under peak load. It can be seen that the general force performance characteristics of each specimen are as follows:

(1) The principal tensile strain and principal compressive strain distribution regularity of concrete are consistent with the test results. The maximum principal tensile strain appears in the AAC blocks near the core column. When the blocks reach the peak tensile strain, two vertical cracks appear in the blocks. Since surface coupling connects the model blocks and the core columns, the constraint effect on the core columns after the cracking of the block is more significant than that in the test.

(2) The compressive strain distribution of the core-column concrete is slight at both ends and significant in the middle along with its height. When the masonry reaches the peak bearing capacity, the restraint of the block in the middle of the core column causes the vertical compressive stress of concrete to exceed its uniaxial compressive strength so that the load-bearing ratio of the concrete core-columns exceeds the calculation results of Formula (3).

(3) When the interfaces between the blocks are in full contact, the vertical compressive stress distribution in the block is not uniform. The maximum vertical compressive stress appears at the end of the block and near the core columns. Such stress distribution characteristics are consistent with the failure pattern of the specimens in Fig. 8.

5.2 Analysis of the Shear Performance of Specimens

According to the shear mechanism analysis in Sect. 2.3, the core columns and the AAC blocks work well together in the early stress stage. When the horizontal crack occurs in the blocks, the larger blocks on both sides bend outwards. Simultaneously, the core columns are subjected to flexural deformation under transverse load, which causes significant compressive stress and uneven compression deformation of the AAC hole wall near the two vertical gaps. As the shear span rate of the core column escalates, the stress mode of the core column gradually develops from shear at the initial stage of loading to bending-shear near the failure stage. To accurately reflect the mechanical characteristics of CNACBM, the finite element analysis model is established in the following way:

(1) The connection of AAC blocks and concrete columns is a crucial factor for the accuracy of the simulation. Triller et al. (2018) got a good research result when they introduced tie connection in analyzing masonry buildings built of low compressive strength units. Ma et al. (2018) employed ABAQUS/Standard to simulate the test process of the RC Frame system with concrete poured into the hollow of wall masonry bricks. The

model ignored the bond-slip between contact surfaces, and parts were tied together in the modules. Since the middle part of the core column is symmetrically stressed and bonded well to the AAC blocks, the connection between the column and the intermediate block is set as the tie constraint and the core columns and outer blocks are in surface-to-surface contact. On the ground of evidence that the core columns separate from the blocks in the late stage of loading at the point of trisection position, the analytical model assumes no restraint in the area of a length of 25 mm on both sides of the vertical joint of the masonry between the blocks and core columns.

(2) To achieve acceptable calculation accuracy (Kwasniewski 2013) while minimizing time cost, the C3D8R (an 8-node linear brick with reduced integration and hourglass control) is applied for both the core column and the block.

The comparison of the peak loads of shear specimens and test average loads is shown in Table 10. The rates between them indicate that the shear capacity obtained by the analytical model aligns well with the experimental results. Figure 15 shows the strain pattern of specimen SK1 under peak load, from which we can see that:

(1) The maximum principal tensile strain of the masonry appears on the outer surface of the left and right blocks near the core columns. The block first has lateral cracks at this position. The continuous development of the cracks causes the outer blocks to bend and deform around the central horizontal joint, which causes the support position of the core column on the outer block to move outward and the shear span rate to increase.

(2) The core column is subjected to bending moment and shearing force at the sections of two vertical joint positions. The local compressive stress transmitted on the blocks by the core column causes local compression deformation. Therefore, the sheer span rate of the core column is further increased in this section, causing the dislocation, deformation, and the ultimate shear failure of the core column.

The stress deformation characteristics and failure modes of the above blocks and core columns are consistent with the experimental results, indicating that the analytical model can provide a superior simulation of the shear performance of the specimens.

6 Conclusions

This paper presented the experimental and analytical research on the core-column non-mortar aerated concrete block masonry, which studied the construction technologies and mechanical properties. The research includes four parts: (a) masonry construction technology; (b) the compressive strength, deformation performance, and compression mechanism of the masonry; (c) the shear strength and shear mechanism of the masonry and (d) the numerical simulation analysis of compression and shear specimens. The major findings and the conclusions of the research are:

1. The concrete core-columns have a significant effect on the integrity and mechanical properties of the masonry. The cancellation of the mortar joints also contributes to efficient and straightforward construction and stable masonry qualities.
2. The strength grades of core-column concrete and AAC block and hole ratio in blocks are critical features that affect the compression capacity of masonry because core columns and blocks bear the axial pressure together. The vertical cracks in the masonry appeared early due to the closure of the horizontal joint of the blocks. Usually, the load-bearing capacity of the masonry reaches a peak only when the core concrete columns reach peak stress.
3. The concrete core-columns provided most of the shear capacity of masonry. When specimens are subjected to a shear load, the experimental value of the shear strength of masonry is lower than that of the pure shear state of the core column on the ground that the core columns are affected by the combined effect of bending and shear deformation.
4. When applying proper analytical models and parameters, the numerical simulation analysis of finite element can well reflect the mechanical properties of CNACBM in compression and shear.
5. When the strength grade of core-column concrete is C25, and the hole ratio is not less than 8.37%, the compressive strength and shear strength of CNACBM is not less than that of the traditional masonry with strength grade M5 mortar. It proves that the masonry can be widely used as bearing walls in low multi-story building structures and as infilled walls in reinforced concrete or steel structures.
6. When the projects require higher compression and shear strength, effective ways of improving hole ratio, enhancing the strength of core concrete, and placing reinforcements in concrete columns can be adopted. Accordingly, other properties of CNACBM will be improved.

The new construction method presented in this study enriches the structural type of masonry structure. The test results, the calculation formula of compression and shear strength, and the relationship of stress and strain obtained by statistical methodology may serve as the

basis of engineering design and source of numerical analysis tools.

Authors' contributions
TP: conceptualization, methodology, validation, formal analysis; ZD: software, resources, formal analysis, writing—original draft; HZ: writing—review and editing, resources, visualization; SW: resources, rata curation. All authors read and approved the final manuscript.

Authors' information
Tianxiang Pi is Associate Professor in Chongqing University, Civil Engineering College of Chongqing University, ShaZheng Road 174, Shapinba, Chongqing, People's Republic of China.

Zhongheng Du is postgraduate student in Chongqing University, Civil Engineering College of Chongqing University, ShaZheng Road 174, Shapinba, Chongqing, People's Republic of China.

Huchen Zhang is postgraduate student in Chongqing University, Civil Engineering College of Chongqing University, ShaZheng Road 174, Shapinba, Chongqing, People's Republic of China.

Sicheng Wang is postgraduate student in Chongqing University, Civil Engineering College of Chongqing University, ShaZheng Road 174, Shapinba, Chongqing, People's Republic of China.

Funding
The project was supported by the Foundamental Research Funds for the Central Universities (2020CDJ-LHZZ-015); Supported by Natural Science Foundation of Chongqing (cstc2020jcyj-msxmX0038).

Data availability
All data, models, or code that support the findings of this study are available from the corresponding author upon reasonable request. All data, models, and code generated or used during the study appear in the submitted article.

Competing interests
There is no known competing financial interests or personal relationships that could have appeared to influence the work reported in this paper.

Author details
[1] Chongqing University, Civil Engineering College of Chongqing University, ShaZheng Road 174, Shapinba, Chongqing, People's Republic of China. [2] Key Laboratory of NewTechnology for Construction of Cities in Mountain Area (Chongqing University), Ministry of Education, Chongqing 400045, People's Republic of China.

Received: 8 October 2020 Accepted: 12 January 2021
Published online: 10 March 2021

References

B.I.o.A. Design, H.A.D. Institute, Technical specification for application of autoclaved aerated concrete, Industry standard-construction industry, 2008, p. 84P; A5.
Bingel, P., & Bown, A. (2009). *Sustainability of masonry in construction*. Cambridge: Woodhead Publishing.
Bolhassani, M., Hamid, A. A., & Moon, F. L. (2016). Enhancement of lateral in-plane capacity of partially grouted concrete masonry shear walls. *Engineering Structures, 108,* 59–76.
C15.04, Standard Test Method for Diagonal Tension (Shear) in Masonry Assemblages, American Society for Testing and Materials, 2007, p. 5P; A4.
C15.10, Standard Practice for Construction and Testing of Autoclaved Aerated Concrete (AAC) Masonry, American Society for Testing and Materials, 2009, p. 3P; A4.
C27.60, Standard Specification for Autoclaved Aerated Concrete (AAC), American Society for Testing and Materials, 2009, p. 7P; A4.
C.A.C. Association. (2008). Test methods of autoclaved aerated concrete, General Administration of Quality Supervision, Inspection and Quarantine of the People's Republic of China; Standardization Administration of the People's Republic of China p. 20.
Eurocode 6: design of masonry structures. (2012). Part 1: general rules for reinforced and unreinforced masonry structures, Deutsches Institut für Normung e.V., 68P; A4.
Eurocode 8: Design of structures for earthquake resistance (2010). Part 1: General rules, seismic actions and rules for buildings, Deutsches Institut für Normung e.V., 31P;A4.
Fay, L., Cooper, P., & de Morais, H. F. (2014). Innovative interlocked soil–cement block for the construction of masonry to eliminate the settling mortar. *Construction and Building Materials., 52,* 391–395.
Fonseca, F. S., Fortes, E. S., Parsekian, G. A., & Camacho, J. S. (2019). Compressive strength of high-strength concrete masonry grouted prisms. *Construction and Building Materials, 202,* 861–876.
Fudge, C. (2011). Designing with AAC to achieve sustainable houses. *Cement Wapno Beton. Management., 9*(10), 1–1.
Ghazi Wakili, K., Hugi, E., Karvonen, L., Schnewlin, P., & Winnefeld, F. (2015). Thermal behaviour of autoclaved aerated concrete exposed to fire. *Cement and Concrete Composites, 62,* 52–58.
Gokmen, F., Binici, B., Aldemir, A., Taghipour, A., & Canbay, E. (2019). Seismic behavior of autoclaved aerated concrete low rise buildings with reinforced wall panels. *J Bulletin of Earthquake Engineering, 17*(7), 3933.
Huchen, Z. (2017). Experimental Study on Mechanical Properties of Mortarless Aerated Concrete Masonry with Core Columns, Chongqing University.
I.a.Q.o.t.P.s.R.o.C. (2011). General Administration of Quality Supervision, Standard for test method of basic mechanics properties of masonry.
Jerman, M., Keppert, M., Vyborny, J., & Cerny, R. (2013). Hygric, thermal and durability properties of autoclaved aerated concrete. *Construction and Building Materials, 41,* 352–359.
Kalliontzis, D., & Schultz, A. E. (2017). Improved estimation of the reverse-cyclic behavior of fully-grouted masonry shear walls with unbonded post-tensioning. *Engineering Structures, 145,* 83–96.
Kwasniewski, L. (2013). Application of grid convergence index in FE computation. *Bulletin of the Polish Academy of Sciences-Technical Sciences, 61*(1), 123–128.
Laukaitis, A., & Fiks, B. (2006). Acoustical properties of aerated autoclaved concrete. *Applied Acoustics, 67*(3), 284–296.
Laurent, J. P., & Guerrechaley, C. (1995). Influence of water-content and temperature on the thermal-conductivity of autoclaved aerated concrete. *Materials and Structures, 28*(182), 464–472.
Ma, X., Ma, J., & Yue, Y. (2018). Experimental and numerical investigation on seismic performance of a hybrid RC frame system with stiffened masonry wall. *Journal of Advanced Concrete Technology, 16*(12), 600–614.
Małyszko, L., Kowalska, E., & Bilko, P. (2017). Splitting tensile behavior of autoclaved aerated concrete: comparison of different specimens' results. *Construction and Building Materials, 157,* 1190–1198.
Martinez, M., & Atamturktur, S. (2019). Experimental and numerical evaluation of reinforced dry-stacked concrete masonry walls. *Journal of Building Engineering, 22,* 181–191.
Muszynski, L., & Gulas, S. (2001). Fire resistance and performance of alternative concrete wall systems. *J. Constr Educat, 6*(3), 146–154.
Ngowi, J. V. (2005). *Stability of dry-stack masonry*. Johannesburg: University of Witwatersrand.
Oliveira D.V. (2003). Experimental and numerical analysis of blocky masonry structures under cyclic loading.
Sokairge, H., Rashad, A., & Elshafie, H. (2017). Behavior of post-tensioned dry-stack interlocking masonry walls under out of plane loading. *Construction and Building Materials, 133,* 348–357.
Standard, C. (2009). *Test methods of autoclaved aerated concrete[JGJ/T 11969–2008]*. Beijing (China): Standards Press of China.
Standard, C. (2011). *Code for design of concrete structures (GB 50010–2010)*. Beijing: Standards Press of China.
Standard, C. (2012). *Code for design of masonry structures[GB50003-2011]*. Beijing: Standards Press of China.
Tanner, J. E., Varela, J. L., Klingner, R. E., Brightman, M. J., & Cancino, U. (2005). Seismic testing of autoclaved aerated concrete shearwalls: a comprehensive review. *Aci Structural Journal, 102*(3), 374–382.

Technical specification for application of autoclaved aerated concrete, 2008.
Thanoon, W. A. M., Alwathaf, A. H., Noorzaei, J., Jaafar, M. S., & Abdulkadir, M. R. (2008). Finite element analysis of interlocking mortarless hollow block masonry prism. *Computers & Structures, 86*(6), 520–528.
Triller, P., Tomaževič, M., & Gams, M. (2018). Seismic behaviour of masonry buildings built of low compressive strength units. Bulletin of Earthquake Engineering., *16*(12), 6191–6219.
B. Trunk, G. Schober, A.K. Helbling, F.H. Wittmann, Fracture mechanics parameters of autoclaved aerated concrete. J Cement and Concrete Research, 29(6) (1999):855-9
Wittmann, F. H. (1983). Autoclaved aerated concrete, moisture and properties
Xiangan, W., Jinghai, Y., & Ping, H. (2007). The influence of the moisture content to the physical and mechanical properties of autoclaved aerated. *Concrete, 33*(033), 24–25.
Zahra, T., & Dhanasekar, M. (2018). Characterisation and strategies for mitigation of the contact surface unevenness in dry-stack masonry. *Construction and Building Materials, 169,* 612–628.
Zhang, J., Wang, Q., Hu, S., & Wang, C. (2008). Parameters verification of concrete damaged plastic model of ABAQUS. *Building Structure., 38*(8), 127–130.
Zhenhai, G. (1999). *Principle of reinforced concrete*. Beijing: Architectural Industry Press.
Zhou, Q., Zhu, F., Yang, X., Wang, F. L., Chi, B., & Zhang, Z. M. (2017). Shear capacity estimation of fully grouted reinforced concrete masonry walls using neural network and adaptive neuro-fuzzy inference system models. *Construction and Building Materials, 153,* 937–947.

Publisher's Note